

Nonlinear effects of hydration on high-pressure sound velocities of rhyolitic glasses

JESSE T. GU^{1,†}, SUYU FU¹, JAMES E. GARDNER¹, SHIGERU YAMASHITA², TAKUO OKUCHI^{2,‡}, AND JUNG-FU LIN^{1,*}

¹Department of Geological Sciences, Jackson School of Geosciences, The University of Texas at Austin, Austin, Texas 78712, U.S.A.

²Institute for Planetary Materials, Okayama University, Misasa, Tottori 682-0193, Japan

ABSTRACT

Acoustic compressional and shear wave velocities (V_p , V_s) of anhydrous (AHRG) and hydrous rhyolitic glasses (HRG) containing 3.28 wt% (HRG-3) and 5.90 wt% (HRG-6) total water concentration (H_2O_i) have been measured using Brillouin light scattering (BLS) spectroscopy up to 3 GPa in a diamond-anvil cell at ambient temperature. In addition, Fourier-transform infrared (FTIR) spectroscopy was used to measure the speciation of H_2O in the glasses up to 3 GPa. At ambient pressure, HRG-3 contains 1.58 (6) wt% hydroxyl groups (OH^-) and 1.70 (7) wt% molecular water (H_2O_m) while HRG-6 contains 1.67 (10) wt% OH^- and 4.23 (17) wt% H_2O_m where the numbers in parentheses are $\pm 1\sigma$. With increasing pressure, very little H_2O_m , if any, converts to OH^- within uncertainties in hydrous rhyolitic glasses such that HRG-6 contains much more H_2O_m than HRG-3 at all experimental pressures. We observe a nonlinear relationship between high-pressure sound velocities and H_2O_i , which is attributed to the distinct effects of each water species on acoustic velocities and elastic moduli of hydrous glasses. Near ambient pressure, depolymerization due to OH^- reduces V_s and G more than V_p and K_s . V_p and K_s in both anhydrous and hydrous glasses decrease with increasing pressure up to ~ 1 – 2 GPa before increasing with pressure. Above ~ 1 – 2 GPa, V_p and K_s in both hydrous glasses converge with those in AHRG. In particular, V_p in HRG-6 crosses over and becomes higher than V_p in AHRG. HRG-6 displays lower V_s and G than HRG-3 near ambient pressure, but V_s and G in these glasses converge above ~ 2 GPa. Our results show that hydrous rhyolitic glasses with ~ 2 – 4 wt% H_2O_m can be as incompressible as their anhydrous counterpart above ~ 1.5 GPa. The nonlinear effects of hydration on high-pressure acoustic velocities and elastic moduli of rhyolitic glasses observed here may provide some insight into the behavior of hydrous silicate melts in felsic magma chambers at depth.

Keywords: Hydrous glass, sound velocity, elasticity, water, rhyolite, Brillouin light scattering spectroscopy, FTIR spectroscopy, high pressure, diamond-anvil cell

INTRODUCTION

Igneous activity at Earth's surface significantly affects society and also shapes the physical and chemical properties of the crust (Carn et al. 2009). The role of "water" in igneous processes is a topic of great interest due to the widespread occurrence of H_2O in Earth's crust and mantle (Mysen and Richet 2005). H_2O is present in magmas and quenched silicate glasses as both molecular water (H_2O_m) and hydroxyl groups (OH^-), where OH^- depolymerizes the silicate network (Stolper 1982a, 1982b). Even at low concentrations, incorporation of these H_2O species has been shown to significantly alter the physical properties of glasses and melts, such as acoustic velocities and elastic moduli (Malfait et al. 2011; Whittington et al. 2012), melting temperature (Kushiro et al. 1968; Grove et al. 2012), density (Richet and Polian 1998; Ochs and Lange 1999; Richet et al. 2000), viscosity (Hess and Dingwell 1996; Richet et al. 1996; Whittington et al. 2000; Hui and Zhang 2007), chemical diffusivities (Behrens and

Zhang 2001), and electrical conductivity (Ni et al. 2011; Guo et al. 2016). These effects are manifested in explosive volcanic eruptions, some of the largest of which involve felsic magmas. The intensity of volcanic eruptions is largely governed by the viscosity of constituent magmas and, correspondingly, the degree to which the magmas are polymerized or depolymerized due to the presence of water species. While H_2O incorporated in silicate melts as OH^- depolymerizes the silicate network and decreases the viscosity of respective melts, it still plays an important role in explosive eruptions (Shaw 1963). H_2O solubility decreases during magma ascent and results in the exsolution of species into molecular H_2O vapor, which expands rapidly at magmatic temperatures (Moore et al. 1995). This process, in combination with the inherently high viscosity of anhydrous felsic magmas, causes the explosiveness of felsic, H_2O -rich magmas (Shaw 1972).

Felsic eruptions can occur when differentiation of partially melted lower crustal materials produce melts with high silica contents (Borg and Clyne 1998). These melts have been reported to contain as much as ~ 6 – 8 wt% H_2O_i at ~ 200 – 400 MPa and ~ 400 – 600 °C (Lowenstern 1994; Wallace et al. 1999; Wallace 2005). Some of the largest felsic eruptions are supervolcanic eruptions that formed the Long Valley and Yellowstone calde-

* E-mail: afu@jsg.utexas.edu

† Orcid 0000-0002-6625-6346

‡ Present address: Institute for Integrated Radiation and Nuclear Science, Kyoto University, Kumatori, Osaka 590-9494, Japan.

ras (Bailey et al. 1976; Croweller et al. 2012). Others felsic eruptions occur along subduction zones, like in the Andes, Japan, and the Cascades (Wallace 2005; Kimura et al. 2015; Brandmeier and Wörner 2016). Although seismic observations can give insight into pre-eruptive processes, the detection and estimation of crustal melt volumes and volatile contents under extreme pressure-temperature (P - T) conditions remain challenging (Flinders and Shen 2017; Flinders et al. 2018). Understanding the acoustic velocities in glasses of relevant compositions and the role of different species of H_2O on altering these velocities with depth can aid in constraining and interpreting melt fractions and volatile contents of magmatic bodies observed from seismic studies. Furthermore, uncovering physical properties, such as density and incompressibility, of rhyolitic melts at depth is essential to our interpretation of eruptive processes, such as melt buoyancy and melt migration.

Two previous studies have focused on the effect of H_2O on the elastic properties of quenched haplogranitic and rhyolitic glasses at ambient pressure (Malfait et al. 2011; Whittington et al. 2012). Other experimental studies have explored the elastic properties of anhydrous silicate glasses of various compositions at high pressure (Meister et al. 1980; Suito et al. 1992; Zha et al. 1994; Sanchez-Valle and Bass 2010; Yokoyama et al. 2010; Liu and Lin 2014; Clark et al. 2016). These studies have shown that silicate glasses exhibit anomalous elastic properties with increasing pressure. In crystalline materials, acoustic velocities and elastic parameters normally increase approximately linearly with pressure. In silicate glasses, however, these properties decrease with pressure up to ~ 2 – 5 GPa, but then increase with pressure above a certain transition pressure. This minima in elastic properties has been attributed to the anomalous compression mechanisms in silicate glasses, whereby densification results from tightening of inter-tetrahedral bond angles and a distortion of the tetrahedral network rather than by decreasing bond lengths (Clark et al. 2014; Wang et al. 2014). The minima in velocities and compressibility correspond to pressures at which silicate glasses reach a packing limit. At higher pressures, densification occurs through shortening of bond lengths and increasing Al and Si coordination. The pressure dependence of the increasing coordination depends upon the composition and polymerization of the glass (Lee et al. 2004, 2011; Lee and Stebbins 2009). The presence of volatiles in interstitial voids can affect the velocity minima and the transition pressure of the glass (Clark et al. 2016). Therefore, the linear effects of water on acoustic velocities of hydrous glasses observed near ambient pressure in previous studies (Malfait et al. 2011; Whittington et al. 2012) may not hold at high pressure and need to be investigated.

The polymerization of hydrous rhyolitic melts and glasses may also change if the proportion of OH^- to H_2O_m changes as a function of pressure and temperature. The relative proportion of H_2O_m and OH^- has been shown to change above ~ 1.0 GPa and could alter the structure and elastic properties of hydrous glasses and melts at higher pressures (Ihinger et al. 1999; Hui et al. 2008; Malfait et al. 2012; Ardia et al. 2014; Helwig et al. 2016). With increasing temperature, the ratio of OH^- to H_2O_m will increase, and OH^- will dominate at magmatic temperatures (Stolper 1982a; Keppler and Bagdassarov 1993; Nowak and Behrens 1995; Shen and Keppler 1995). Because studying the

properties of melts at high pressure and temperature conditions remains challenging, silicate glasses have commonly been used as analogs for silicate melts (Williams and Jeanloz 1998; Lee et al. 2008). Previous studies have shown that quenched glasses retain the local structure of their corresponding liquids (Seifert et al. 1981; Malfait et al. 2014), which has been commonly used as justification for the analog approach.

Despite previous efforts, the effects of H_2O_m and OH^- on the acoustic velocities and elastic moduli of rhyolitic glasses at pressures above a few hundred megapascals have been poorly studied. At pressures relevant to felsic magma chambers, elastic properties depend not only on H_2O_v , but also on how the different species of H_2O interact with the structure of the glass. The linear hydration effect on acoustic velocities of rhyolitic glasses observed previously at ambient pressure (Malfait et al. 2011; Whittington et al. 2012) could become nonlinear at high pressures. To better understand the behavior of felsic magmas at depth, it is thus essential to constrain water speciation in hydrous glasses and correlate these species with experimental acoustic velocities and elastic moduli at high pressures.

Here, we report acoustic velocities and elastic moduli in both anhydrous (AHRG) and hydrous rhyolitic glasses (HRG) containing 3.28 wt% H_2O_i (HRG-3) and 5.90 wt% H_2O_i (HRG-6), measured using Brillouin light scattering (BLS) spectroscopy in a diamond-anvil cell (DAC) up to 3 GPa. Complementary FTIR measurements were also conducted to examine H_2O speciation as a function of pressure. These observations are applied to correlate how the different species of H_2O contribute to the observed changes in velocities and equation of state parameters of hydrous rhyolitic glasses at high pressures. We observe nonlinear effects of hydration on acoustic velocities and elastic moduli at high pressure, which are applied to decipher elastic behaviors of felsic magmas in the deep crust.

EXPERIMENTAL METHODS

Rhyolitic glass samples were cored from a natural obsidian, which consisted of high-silica rhyolitic glass and <1 vol% microlites of Fe-Ti oxides (Gardner and Ketcham 2011). Two cores were placed in Au capsules, along with a pre-determined amount of deionized water to ensure H_2O -saturation at run conditions. The capsules were welded shut and then heated and weighed to ensure that no leaks existed. The samples were then run in externally heated pressure vessels at high- P - T conditions for ~ 7 days in the Petrology Laboratory of the University of Texas at Austin (Table 1). A third core was placed inside a Pt capsule for the synthesis of anhydrous rhyolitic glass (AHRG), which was left open, and was placed inside an externally heated pressure vessel and run at 0.5 MPa and 1150 °C in Ar gas to dehydrate the glass sample. All samples were quenched rapidly, and the two runs at elevated pressures were weighed to check for leaks. After quenching, sample compositions and homogeneity were evaluated by the JEOL JXA-8200 Electron Microprobe in the Department of Geological Sciences at The University of Texas at Austin (Table 2). At least 10 measurements of each glass sample were made with an accelerating voltage of 10 kV, beam currents of 2–10 nA, and defocused beam sizes of 10–20 μm . Oxide compositions were averaged and normalized to 100% for comparison among different glass samples (Table 2). In total, three samples were synthesized and used for the study: one glass with 3.28 wt% H_2O_i (HRG-3) and one glass with 5.90 wt% H_2O_i (HRG-6), while the third core produced anhydrous glass with ~ 0.1 wt% H_2O_i (AHRG) (Table 1).

TABLE 1. Synthesis conditions of rhyolitic glasses

Sample	Run	P (MPa)	T (°C)	Time (h)	OH^- (wt%)	H_2O_m (wt%)	H_2O_i (wt%)
HRG-6	G-1730	190	850	169	1.67 (10)	4.23 (17)	5.90 (20)
AHRG	G-1756	0.5	1150	41.5	–	–	<0.15
HRG-3	G-1800	67.5	875	165	1.58 (6)	1.70 (7)	3.28 (9)

Note: Values in parentheses are standard deviations ($\pm 1\sigma$) from FTIR measurements.

TABLE 2. Compositions and total water contents (H_2O_t) of glasses in this study

Oxide wt%	Whole-rock	AHRG	HRG-3	HRG-6
SiO ₂	76.53	76.70(98)	76.23(67)	76.46(97)
Al ₂ O ₃	13.01	13.30(18)	13.37(19)	13.23(22)
Na ₂ O	3.87	4.00(40)	3.67(3)	3.85(17)
K ₂ O	4.91	4.85(21)	4.99(7)	4.91(10)
CaO	0.74	0.82(5)	0.77(3)	0.75(3)
FeO	0.79	0.23(14)	0.84(10)	0.67(9)
MgO	0.02	0.03(2)	0.02(1)	0.02(2)
MnO	0.08	0.02(2)	0.05(1)	0.06(2)
TiO ₂	0.06	0.04(3)	0.05(3)	0.05(2)
H ₂ O _t	–	<0.15	3.28(9)	5.90(18)

Notes: The sum of components other than H₂O_t are normalized to 100% for comparison between different glass samples. Values in parentheses are standard deviations ($\pm 1\sigma$) from EPMA and FTIR measurements.

FTIR analyses of double-polished samples at ambient conditions were carried out on all glass samples in the Department of Geological Sciences at The University of Texas at Austin to determine H₂O_t using a Thermo-Electron Nicolet 6700 spectrometer and Continuum IR microscope. Absorbances in the near-infrared region at ~4500 and ~5200 cm⁻¹ were used to calculate H₂O_t at ambient conditions following the procedures of Gardner and Ketcham (2011). At ambient pressure, AHRG contains ~0.1 wt% H₂O_t, HRG-3 contains 1.58(6) wt% OH⁻ and 1.70(7) wt% H₂O_m, and HRG-6 contains 1.67(10) wt% OH⁻ and 4.23(17) wt% H₂O_m. The water content in AHRG is negligible compared to the two hydrous glasses so it is used as the reference for the anhydrous rhyolitic glass.

Furthermore, densities at ambient pressure (ρ_0) for the glasses were determined from the partial molar volumes of oxide components and H₂O at 300 K following literature procedures (Richet et al. 2000; Lin and Liu 2006). Archimedes's method with toluene as the immersion liquid was used to confirm that the density of HRG-6 matched the calculated density within uncertainties. The other two glass samples, AHRG and HRG-3, were not checked with this method because of insufficient quantities of materials.

Two runs of micro-FTIR measurements at high pressure were carried out on all glass samples in DACs at the Institute for Planetary Materials, Okayama University in Misasa, Japan. Micro-FTIR measurements were taken using a Jasco FTIR-6200 Fourier-transform spectrometer fitted with a Jasco IRT-7000 microscope with Cassegrain optics (Chertkova and Yamashita 2015). Transmitted light was received by a LN₂-cooled HgCdTe detector for both mid-infrared (MIR) and near-infrared (NIR) measurements. Analytical procedures were similar to those described in Chertkova and Yamashita (2015), except a CaF₂/Si beamsplitter was used for NIR measurements while a KBr/Ge beamsplitter was used for MIR measurements. Glass sample platelets were prepared by polishing both sides using 3M diamond films with 1 and 0.3 μ m grain sizes. Ambient-pressure spectra in the NIR region were recorded to confirm H₂O_t in the glasses and to compare with MIR spectra before high-pressure runs (Fig. 1). H₂O speciation in HRG-6 calculated using MIR and NIR spectra agreed well within uncertainties. In high-pressure measurements, background spectra of the diamond anvils and the sample chamber were taken prior to each measurement and were subsequently subtracted from the recorded spectra (Chertkova and Yamashita 2015). In the first run (FTIR-Run 1), a 250 μ m thick Re gasket with a 300 μ m hole in the center was pre-indented to a thickness of ~100 μ m and was sandwiched between diamond anvils with diameters of 600 μ m in a DAC. One piece of AHRG that was 23 \pm 3 μ m thick and one piece of HRG-6 that was 28 \pm 3 μ m thick were simultaneously loaded into the DAC along with Ne and a ruby sphere as a pressure medium and pressure calibrant, respectively (Dewaele et al. 2008). The MIR region from 1400–4000 cm⁻¹ was used in this run to measure H₂O_t and H₂O_m in the glasses (Fig. 1). OH⁻ contents were then calculated based on the difference between H₂O_t and H₂O_m. In the second run (FTIR-Run 2), a DAC with a pair of 750 μ m culets was equipped with a 500 μ m thick Re gasket pre-indented to ~400 μ m with a 650 μ m hole in the center. A 333 \pm 3 μ m thick piece of HRG-3 was loaded into the DAC along with Ne and a ruby sphere. The large thickness of the sample resulted in saturated absorption bands in the MIR region, so bands in the NIR region from 4000–6000 cm⁻¹ were used to measure H₂O speciation instead (Fig. 1).

Three separate runs of BLS measurements were carried out on the glasses up to 3 GPa in DACs (Fig. 2). Each DAC with a pair of 600 μ m culets was equipped with a 250 μ m thick Re gasket pre-indented to ~150 μ m with a 300 μ m hole in the center. Glass samples with diameters of ~100 μ m were double-polished down to <70 μ m thick using 3M diamond films with 1 and 0.3 μ m grain sizes. The samples were then placed in a sample chamber with either Ne or 4:1 methanol:ethanol as the

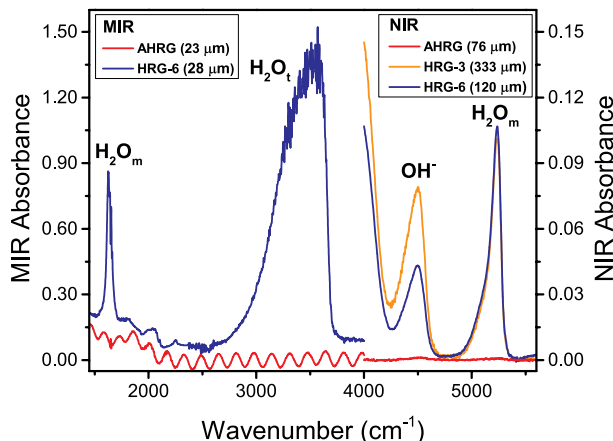


FIGURE 1. Representative raw FTIR spectra of rhyolitic glasses at ambient conditions. Numbers in parentheses represent sample thicknesses. The absorption bands are assigned and labeled with the associated H₂O species based on previous studies (Stolper 1982b; Newman et al. 1986; Withers and Behrens 1999). MIR spectra (<4000 cm⁻¹) were only recorded for thin samples (<~30 μ m), whereas NIR spectra (>4000 cm⁻¹) allow for comparison between thicker samples. The modulations in the MIR spectrum of AHRG are fringes resulting from the double-side polished sample. (Color online.)

pressure medium (Fig. 2). It has been proposed that the use of noble gas pressure media could alter the compressibilities and measured velocities in silicate glasses (Shen et al. 2011; Weigel et al. 2012; Clark et al. 2014; Coasne et al. 2014), so 4:1 methanol:ethanol was used as the pressure medium in a separate run to check for these effects. Both AHRG and HRG-6 were loaded simultaneously in the first (BLS-Run 1) and second (BLS-Run 2) runs with Ne and 4:1 methanol:ethanol, respectively. In the third run (BLS-Run 3), HRG-3 was loaded with Ne as the pressure medium. In all runs, a ruby sphere was used as the pressure calibrant (Dewaele et al. 2008).

BLS measurements were taken at the Mineral Physics Laboratory in the Department of Geological Sciences at The University of Texas at Austin. The Brillouin system is equipped with a 532 nm Coherent Verdi V2 laser and a JRS six-pass tandem Fabry-Perot interferometer (Lu et al. 2013; Yang et al. 2014; Fu et al. 2017). The focused beam size at the sample position was ~30 μ m. Spectra were collected in a symmetric forward scattering geometry with an external angle of 48.1°. The system is calibrated monthly using standard distilled water and silica glass (Lu et al. 2013). Acoustic velocities were calculated from the measured frequency shift from:

$$V_{P,S} = \frac{\Delta\nu_B \lambda_0}{2 \sin(\theta/2)}$$

where $V_{P,S}$ is the compressional (V_P) or shear (V_S) velocity, $\Delta\nu_B$ is the measured Brillouin shift, λ_0 is the laser wavelength in vacuum (approximately the same as in air) (532 nm), and θ is the external scattering angle (48.1°). Representative Brillouin spectra of rhyolitic glasses at high pressure are shown in Figure 2. See Online Material¹ for data.

DATA ANALYSIS AND MODELING

Measured acoustic velocities from BLS were used to derive other elastic parameters, including density (ρ), adiabatic bulk moduli (K_S), and shear moduli (G) (Sanchez-Valle and Bass 2010; Liu and Lin 2014). To derive these elastic moduli from velocity data, it is first necessary to determine the density of the glasses as a function of pressure. Assuming the glass samples behave elastically under compression, the density of the glasses at high pressures can be derived from:

$$\rho - \rho_0 = \int_{P_0}^P \frac{1}{\left(V_P^2 - \frac{4}{3} V_S^2 \right)} dP$$

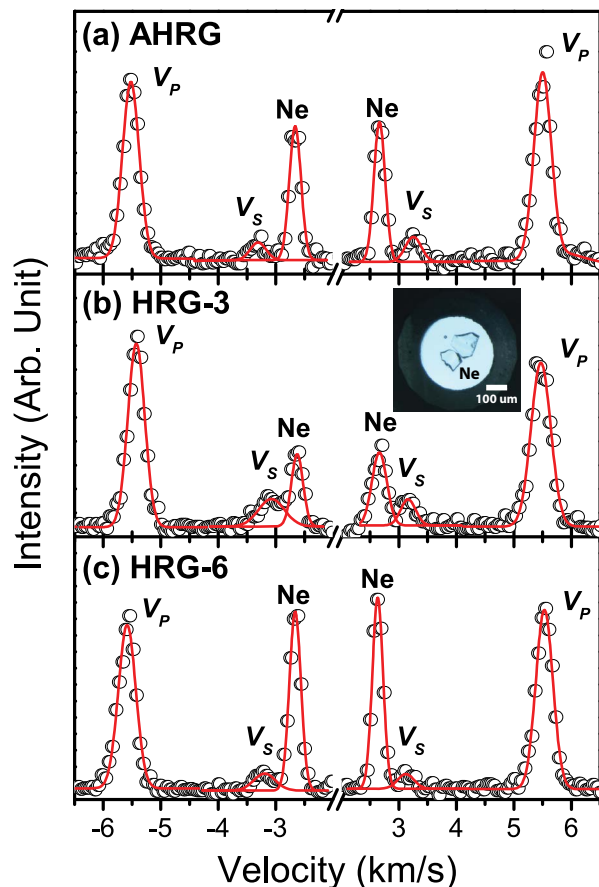


FIGURE 2. Representative Brillouin Light Scattering spectra of rhyolitic glasses at ~3 GPa. (a) anhydrous (AHRG) and (b) and (c) hydrous glasses with 3.28 wt% H₂O_i (HRG-3) and 5.90 wt% H₂O_i (HRG-6). Open circles are experimental data and red lines show fitted Gaussian peaks. The compressional (V_p) and shear (V_s) wave velocities of the glasses and Ne are labeled. The insert in **b** shows the sample chamber in a DAC that has been loaded with AHRG (lower left), HRG-6 (upper right), ruby as the pressure calibrant (upper left), and Ne as the pressure medium. (Color online.)

where ρ is the density of the glass at high pressure, ρ_0 is the density of the glass at ambient pressure (0.1 MPa), and P is the pressure (Sanchez-Valle and Bass 2010; Liu and Lin 2014; Sakamaki et al. 2014). Once acoustic velocities and densities at corresponding pressures were determined, the elastic moduli were determined from:

$$K_s = \rho \left(V_p^2 - \frac{4}{3} V_s^2 \right)$$

$$G = \rho V_s^2$$

Fourth-order Eulerian finite-strain EoS (Birch 1978) were then fit to the derived elastic moduli. The fourth-order EoS was used to better capture the anomalous incompressibility and nonlinear change in K_s and G in silicate glasses with increasing pressure (Clark et al. 2014; Liu and Lin 2014). Fitted elastic moduli are also used to simultaneously fit measured acoustic velocities as a function of pressure up to 3 GPa.

Measured FTIR spectra were analyzed to calculate H₂O speciation of the samples as a function of pressure via the Beer-Lambert law, which relates absorbance and thickness of a material to the concentration of the absorbing species within it (Newman et al. 1986; Ihinger et al. 1999; McIntosh et al. 2017), according to:

$$C_{\text{H}_2\text{O}_{\text{m,OH}}} = \frac{M * A}{\rho * t * \epsilon}$$

where $C_{\text{H}_2\text{O}_{\text{m,OH}}}$ is the concentration of either H₂O_i, H₂O_m, or H₂O dissolved as OH⁻, M is the molar mass of the species of interest, A is the absorbance, ρ is density of the glass, t is thickness of the glass, and ϵ is the molar absorption coefficient of the FTIR band of interest (Fig. 3). ϵ in rhyolitic glasses has been studied extensively in both MIR and NIR regions (Newman et al. 1986; Zhang et al. 1997; Withers et al. 1999; McIntosh et al. 2017). Both MIR and NIR calibrations result in the same H₂O speciation, within uncertainties, in HRG-6 at ambient pressure. Therefore, both IR regions are suitable for calculation of H₂O speciation at high pressure. Densities of glass samples as a function of pressure were determined from equation of state (EoS) fitting. Because glass is elastically isotropic, the thickness of a sample at high pressure is determined from:

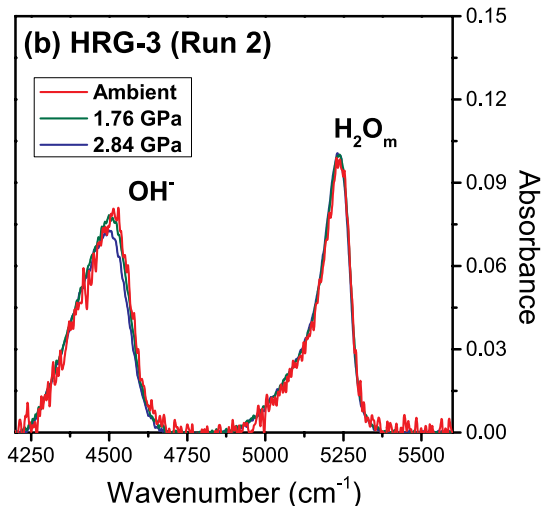
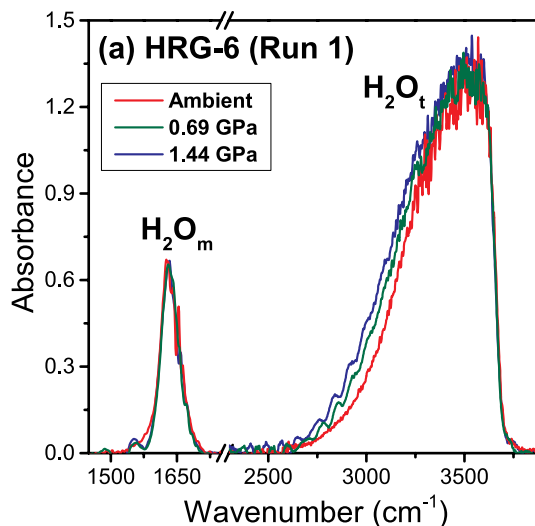


FIGURE 3. Representative FTIR spectra of the two hydrous rhyolitic glasses with increasing pressure. (a) FTIR spectra of HRG-6 (5.90 wt% H₂O_i) in the mid-IR region. (b) FTIR spectra of HRG-3 (3.28 wt% H₂O_i) in the near-IR region. Linear baselines were subtracted from the mid-IR spectra in **a**, whereas flexicurve baselines were used for background subtraction from the near-IR spectra in **b** (Newman et al. 1986; Withers and Behrens 1999; McIntosh et al. 2017). Ne was used as the pressure medium in FTIR experiments. (Color online.)

$$t = t_0 \sqrt{\frac{\rho_0}{\rho}}$$

where t_0 is the sample thickness in μm at ambient pressure that was measured using an optical microscope (Amin et al. 2012). The MIR region was used to determine the H_2O speciation in HRG-6. The area under the peaks at ~ 1600 and $\sim 3500\text{ cm}^{-1}$ was determined after a linear baseline was subtracted from the raw spectra (Newman et al. 1986). The species-dependent method of determining H_2O from the band at $\sim 3500\text{ cm}^{-1}$ was used along with molar absorption coefficients from Newman et al. (1986) and McIntosh et al. (2017). Because of the thickness of HRG-3, the bands in the MIR region were saturated. The ~ 4500 and $\sim 5200\text{ cm}^{-1}$ peaks in the NIR region were therefore used instead to determine H_2O speciation. However, the sample was bridged and crushed by the diamond anvils at $\sim 1.5\text{ GPa}$, so no spectra were recorded above this pressure. Using published values for the molar absorption coefficients, the speciation of H_2O_m and OH^- were determined from the area under the peaks at ~ 4500 and $\sim 5200\text{ cm}^{-1}$ after a flexicurve baseline was subtracted from the raw spectra (Fig. 3) (Withers and Behrens 1999).

RESULTS

Analyses of BLS and FTIR results show that the addition of H_2O into rhyolitic glasses decreases V_p and V_s in hydrous glasses at ambient pressure, consistent with previous studies (Fig. 4) (Malfait et al. 2011; Whittington et al. 2012). Compared to AHRG at ambient pressure, V_p (V_s) in HRG-3 and HRG-6 are reduced by $\sim 4.8\%$ ($\sim 6.7\%$) and $\sim 5.1\%$ ($\sim 8.6\%$), respectively (Table 3). Our results are consistent with those of rhyolitic glasses in previous studies and show slightly larger reductions in velocities compared to haplogranitic glasses (Meister et al. 1980; Suito et al. 1992; Malfait et al. 2011; Whittington et al. 2012). In addition, reductions in velocities due to hydration are larger in V_s than those in V_p . The larger reductions in V_s can be attributed to depolymerization of the glass structure by OH^- , which reduces its shear-resistance (Stolper 1982b, 1982a; Deschamps et al. 2011). V_p , on the other hand, is not affected as much because the bulk

TABLE 3. Ambient-pressure acoustic velocities, elastic moduli, and densities of investigated glasses

	AHRG (BLS-Run 1)	HRG-3 (BLS-Run 3)	HRG-6 (BLS-Run 1)
V_p (km/s)	5.87(3)	5.59(3)	5.57(3)
V_s (km/s)	3.63(3)	3.38(3)	3.32(3)
K_s (GPa)	39.7(3)	36.9(4)	37.2(4)
K_s' (no unit)	-3.7(3)	-1.4(6)	-2.2(4)
K_s'' (GPa^{-1})	1.9(1)	1.7(3)	2.2(2)
G (GPa)	31.0(2)	26.6(2)	25.0(2)
G' (no unit)	-1.7(2)	-1.4(3)	-1.5(2)
G'' (GPa^{-1})	0.4(1)	0.6(2)	1.1(1)
Density (g/cm^3)	2.353(5)	2.318(5)	2.270(5)

Notes: Values in parentheses are estimated uncertainties for velocities and densities, or standard deviations ($\pm 1\sigma$) from equation of state fitting for elastic moduli.

compressibility of the glass structure is not altered as much by H_2O_m in interstitial voids or by depolymerization due to OH^- .

The pressure dependence of H_2O speciation was determined from analyses of high-pressure FTIR spectra (Fig. 3). Spectral features in high-pressure FTIR spectra are generally consistent with those observed at ambient pressure. Broadening of the band at $\sim 3250\text{ cm}^{-1}$, however, is interpreted to result from pressure-induced broadening of the absorption band. Similarly, pressure appears to shift the band at $\sim 4500\text{ cm}^{-1}$ to lower wavenumbers. Despite these slight modifications, calculated H_2O_i remains constant within uncertainties at high pressure. With increasing pressure, very little, if any, H_2O_m in HRG-6 appears to be converted into OH^- (Fig. 5). Conversion of water species is not resolvable due to the large uncertainties in our calculated species abundances. If present, this conversion mostly occurs below 1.5 GPa in HRG-6. In glasses with low H_2O_i ($< 4\text{ wt}\%$), the conversion from H_2O_m to OH^- has only been observed above 1 GPa in previous studies (Hui et al. 2008). In contrast, HRG-3 shows almost no change in speciation up to $\sim 1.5\text{ GPa}$ (Fig. 5).

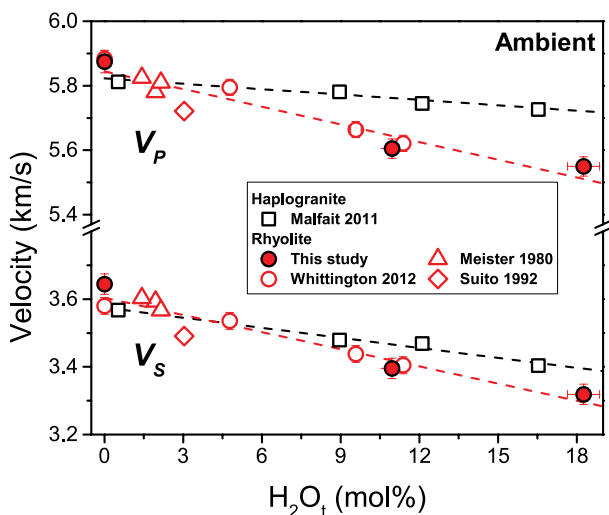


FIGURE 4. Comparison of acoustic velocities in rhyolitic and haplogranitic glasses as a function of total water content (H_2O_i) at ambient conditions. Red symbols represent acoustic velocities in rhyolitic glasses whereas open black symbols represent acoustic velocities in haplogranitic glasses. The dashed red lines are linear fits to the data for rhyolitic glasses while the dashed black lines are linear best-fit lines for haplogranitic glasses similar to those used by Malfait et al. (2011). Uncertainties are smaller than symbols when not shown. (Color online.)

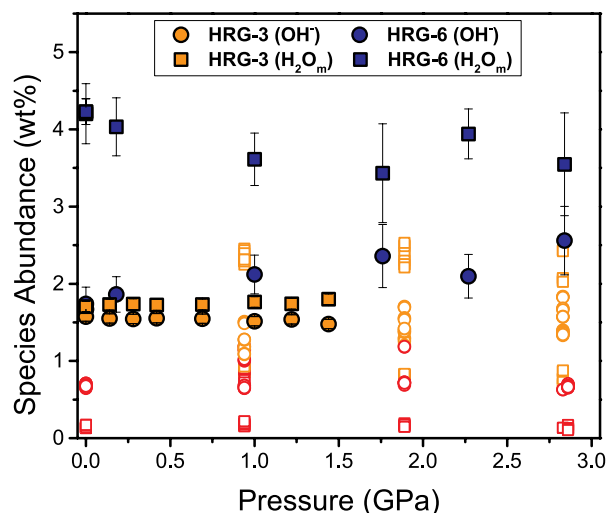


FIGURE 5. Calculated H_2O speciation in the two hydrous rhyolitic glasses (HRG-3 and HRG-6). Abundance of hydroxyl groups (OH^-) is depicted by circles while abundance of molecular water (H_2O_m) is depicted by squares. Error bars are shown for HRG-6 (5.90 wt% H_2O_i) whereas they lie within the symbols for HRG-3 (3.28 wt% H_2O_i). Literature data from (Hui et al. 2008) are shown as open symbols where red symbols indicate glasses with $< 2\text{ wt}\%$ H_2O_i , and orange symbols represent glasses with 2–4.16 wt% H_2O_i . (Color online.)

Even if HRG-3 undergoes changes in speciation above ~ 1.5 GPa, as reported in the literature, the quantity of change will not be large and the relative ratio of OH^- to H_2O_m will remain relatively constant. At all pressures, HRG-6 will contain more than a factor of two more H_2O_m than HRG-3, whereas their OH^- contents will remain similar. Therefore, differences in behavior between HRG-3 and HRG-6 can almost entirely be attributed to the excess H_2O_m in HRG-6. These samples allow us to investigate the effects of water species on velocities and elastic moduli of rhyolitic glasses at high pressure without having to consider changes in speciation.

Measured V_p and V_s of the three glasses display nonlinear and negative slopes with increasing pressure up to $\sim 1\text{--}2$ GPa (Fig. 6). V_s in HRG-6 shows a minimum and increases above ~ 2 GPa, whereas V_s in both AHRG and HRG-3 decrease throughout the whole experimental pressure range. On the contrary, there is a minimum in V_p below 3 GPa in all glass samples. The anomalous pressure dependence of velocities is consistent with previous studies on silicate glasses (Sanchez-Valle and Bass 2010; Clark et al. 2014; Liu and Lin 2014). The pressure at which acoustic velocities reach their minima in glasses is termed in the literature as the “transition” pressure and has been shown to occur at lower pressures due to the presence of volatiles (Weigel et al. 2012; Coasne et al. 2014; Liu and Lin 2014; Clark et al. 2016). In rhyolitic glasses, this transition pressure decreases in the hydrous glasses, such that the transition in V_p occurs at $\sim 1\text{--}1.5$ GPa in HRG-3 and HRG-6 whereas it occurs at ~ 2 GPa in AHRG. The lower transition pressure in hydrous glasses causes V_p and V_s in hydrous glasses to converge with those in AHRG (Fig. 6c). In other words, velocity differences (ΔV_p and ΔV_s) between hydrous glasses and AHRG become less negative at high pressure. Eventually, V_p in HRG-6 crosses over and becomes higher than V_p in both HRG-3 and AHRG. Based on the modeled velocities, the crossover in V_p between AHRG and HRG-3 occurs above 3 GPa. V_s of HRG-6 converges with that of HRG-3 and eventually becomes indistinguishable from HRG-3 above ~ 2 GPa. Crossovers in V_s between hydrous glasses and their anhydrous counterpart appear to occur above 3 GPa. Despite differences in transition pressures between V_p and V_s , and even though ΔV_s remains $\sim 4\%$ lower than ΔV_p , both ΔV_p and ΔV_s in hydrous glasses display remarkably similar trends at high pressure (Fig. 6c). The convergence of ΔV_p and ΔV_s at different rates between all three samples produces nonlinear effects of hydration at high pressure.

The derived densities of hydrous rhyolitic glasses at ambient pressure are consistent with reported densities of haplogranitic and rhyolitic glasses (Fig. 7) (Malfait et al. 2011; Whittington et al. 2012). These observations show decreasing density with the addition of H_2O_i where increasing H_2O_i by 1 wt% reduces density by $\sim 0.5\text{--}0.6\%$. In contrast, the derived high-pressure densities are higher than those observed in haplogranitic glasses quenched from high pressures and measured at ambient pressure (Ardia et al. 2014). Despite these differences, we observe similar trends in the density differences ($\Delta\rho$) between hydrous glasses and AHRG where the difference in density due to hydration increases above ~ 1.5 GPa (Fig. 7 inset). The modeled elastic moduli of the glasses also show anomalous behavior at high pressure due to hydration and correspond to the density trends above ~ 1.5 GPa (Fig. 8).

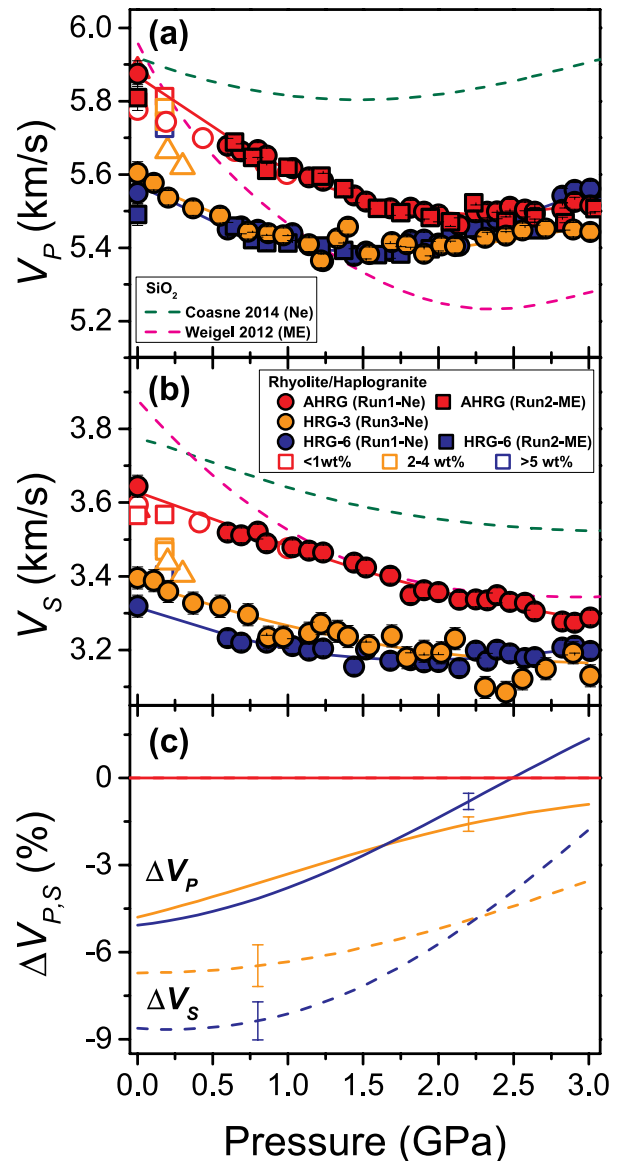


FIGURE 6. Acoustic velocities in anhydrous and hydrous rhyolitic glasses as a function of pressure. (a) Compressional wave velocities (V_p), (b) shear wave velocities (V_s), and (c) percent differences in velocity [$100 \cdot (V_{\text{hydrous}} - V_{\text{anhydrous}}) / V_{\text{anhydrous}}$] between hydrous glasses and the anhydrous glass in this study. In a and b, solid circles are experimental data from BLS-Run 1 and BLS-Run 3 where Ne was used as the pressure medium. Solid squares are experimental data from BLS-Run 2 where 4:1 methanol:ethanol (ME) was used as the pressure medium. Solid lines are modeled velocity profiles using data from the BLS-Run 1 and BLS-Run 3. Open symbols are literature data on haplogranitic or rhyolitic glasses: open squares (Malfait et al. 2011), open circles (Whittington et al. 2012), and open triangles (Meister et al. 1980). Dashed lines are velocity profiles for SiO_2 glasses with either Ne (green, Coasne et al. 2014) or ME (magenta, Weigel et al. 2012) as the pressure medium. In c, solid lines represent percent differences in V_p , dashed lines represent percent differences in V_s , and vertical ticks represent error bars. The color of the lines corresponds to the glass sample they represent (red = AHRG, orange = HRG-3, and blue = HRG-6). (Color online.)

The addition of H₂O decreases both K_S and G below ~1.5 GPa (Table 3). At these pressures, K_S is virtually indistinguishable between HRG-3 and HRG-6, whereas the reduction in G due to hydration between HRG-3 and HRG-6 is discernible. Above ~1–1.5 GPa, K_S in all three glasses converge and become virtually indistinguishable from each other. This convergence causes K_S in hydrous glasses to increase more rapidly than in AHRG and results in a slight increase in $\Delta\rho$ in hydrous glasses (Fig. 7 inset). In G , however, HRG-3 and HRG-6 begin to converge with AHRG above ~2 GPa but remain distinctly lower. It is possible that convergence of G between hydrous glasses and their anhydrous counterpart occur at higher pressures. The pressure-dependence of K_S is more similar to that of V_p , whereas the pressure-dependence of G is more comparable to that of V_s .

Previous studies have reported that the use of noble gases (He or Ne) as pressure media can significantly alter the observed elastic properties in silicate glasses (Shen et al. 2011; Weigel et al. 2012; Clark et al. 2014; Coasne et al. 2014). These effects have been attributed to the adsorption of noble gas molecules into interstitial sites in silicate glasses, which stiffens the glass network, making it more incompressible. The difference between our results using the two pressure transmitting media is, however, much smaller compared to those observed in silica glass at similar pressures (Fig. 6) (Coasne et al. 2014). These differences may be due to the synthesis of our glasses under volatile-rich conditions. According to our velocity results using Ne and 4:1 methanol:ethanol, respectively, we observed little change in velocities below ~2.5 GPa. Above ~2.5 GPa, velocities from the run with Ne as the pressure medium begin to diverge from the velocities from the run where 4:1 methanol:ethanol was used

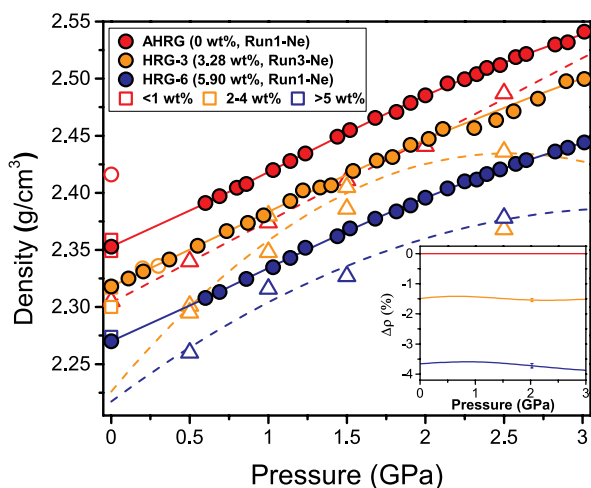


FIGURE 7. Modeled density-pressure relationships of anhydrous and hydrous rhyolitic glasses. Solid symbols represent densities calculated from our measured sound velocities with Ne as the pressure medium. Solid lines are best fits from equation-of-state modeling (Birch 1978). Open symbols are literature data on haplogranitic or rhyolitic glasses: open squares (Malfait et al. 2011), open circles (Whittington et al. 2012), and open triangles (Ardia et al. 2014). Dashed lines are polynomial fits to the data from Ardia et al. (2014). The insert shows modeled percent differences in density [$100 \cdot (\rho_{\text{hydrous}} - \rho_{\text{anhydrous}}) / \rho_{\text{anhydrous}}$] between hydrous glasses and the anhydrous glass in this study. (Color online.)

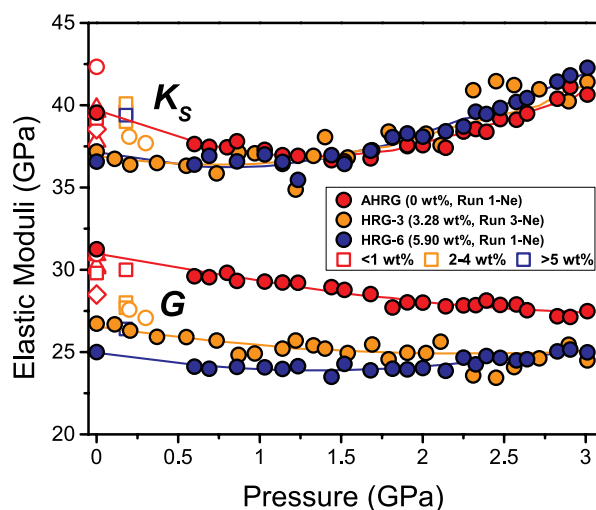


FIGURE 8. Adiabatic bulk moduli and shear moduli of anhydrous and hydrous rhyolitic glasses as a function of pressure. Solid symbols represent elastic moduli calculated from measured sound velocities with Ne as the pressure medium. Solid lines are best fits from equation-of-state fitting (Birch 1978). Uncertainties are smaller than symbols. Open symbols are literature data on haplogranitic or rhyolitic glasses: open squares (Malfait et al. 2011), open circles (Whittington et al. 2012), open triangles (Meister et al. 1980), and open diamonds (Suito et al. 1992). (Color online.)

as the pressure medium. We note that using Ne as the pressure medium may alter the elasticity of glasses at higher pressures in DAC studies, but does not display any noticeable effects on rhyolitic glasses in the pressure range investigated here.

DISCUSSION

At ambient pressure and relatively low pressures (<1 GPa), the incorporation of H₂O species decreases acoustic velocities and elastic moduli because dissolved H₂O is much more compressible than the surrounding silicate network (Figs. 4 and 8) (Richet and Polian 1998). The effects of hydration on V_s are larger than those on V_p due to depolymerization of the glass network due to OH⁻ (Stolper 1982a, 1982b; Deschamps et al. 2011). At higher pressures, interactions between the silicate glass network and H₂O species result in the observed nonlinear trends in sound velocities and elastic moduli. The anomalous pressure dependence of sound velocities in silicate glasses has been attributed to their compression mechanism. Rather than reducing bond lengths, glasses are compressed by the collapse of interstitial void spaces and changing of bond angles between bridging tetrahedra (Weigel et al. 2012; Clark et al. 2014; Wang et al. 2014). The transition at which acoustic velocities reach their minima as a function of pressure has been associated with a tetrahedral packing limit, above which the compression mechanism changes in silicate glasses (Wang et al. 2014). The hydrous glasses in this study have different transition pressures compared to that of AHRG in both V_p and V_s ; the transition pressure appears to decrease with increasing H₂O_i (Fig. 6). The presence of H₂O_m in interstitial sites may contribute to this shift in transition pressure with increasing H₂O_i. The packing limit of

hydrous glasses is reached at lower pressures below ~ 1.5 GPa because H_2O_m in interstitial sites is more compressible than the anhydrous silicate network (Fig. 8). That is, higher quantities of H_2O allow the glass to be compressed more easily at pressures below ~ 1.5 GPa. The transition pressure in V_p occurs below ~ 2 GPa, whereas it occurs above ~ 1.5 – 2 GPa in V_s in all glasses, indicating that G is less responsive to the packing limit in hydrous glasses. While K_S begins increasing in both hydrous glasses at ~ 0.75 GPa, G only begins to increase above ~ 1.5 GPa. Between ~ 0.75 – 1.5 GPa, H_2O_m in interstitial sites prevents compression of the surrounding silicate network and causes K_S in hydrous glasses to converge with K_S in AHRG. Indiscernible K_S values between hydrous and anhydrous glasses above ~ 1.5 GPa indicate that the silicate glass network controls compression at these pressures.

The incorporation of volatiles in interstitial sites has also been shown to flatten the pressure dependence of acoustic velocities (Weigel et al. 2012; Coasne et al. 2014; Clark et al. 2016). Similarly, V_p of hydrous glasses in this study show flatter slopes as a function of pressure below their transition pressures. In contrast, the V_p -pressure slopes are higher in hydrous glasses above their transition pressures. As a result of the lower transition pressure and the steeper V_p -pressure slope above its transition pressure, V_p in HRG-6, which contains abundant H_2O_m , exceeds V_p in both HRG-3 and AHRG above ~ 1.5 GPa (Fig. 6). The more positive slopes and crossover in V_p can be attributed to the presence of H_2O_m in interstitial voids, which causes incompressibility in hydrous glasses to converge with those in AHRG (Fig. 8). Because hydrous glasses are intrinsically less dense than AHRG, their bulk moduli eventually become very similar above their transition pressures. While V_s -pressure slopes among all glasses are relatively similar below ~ 1.5 GPa, V_s in both hydrous glasses converge with AHRG above ~ 1.5 GPa. Based on modeled velocities, it appears that V_s in hydrous glasses will crossover and become higher than those in AHRG above 3 GPa. These results imply that the effects of hydration on acoustic velocities and elastic moduli are nonlinear at high pressures up to 3 GPa.

IMPLICATIONS

The nonlinear effects of H_2O on acoustic velocities and elastic moduli reported here imply that different water species may also alter acoustic velocities and elastic moduli differently at different P - T conditions relevant to felsic magma chambers at depth. These results could thus be used to provide some insight into the behavior of hydrous felsic silicate melts at depth, given that experimental results at such conditions are still not feasible. For example, the nonlinear hydration effects reported here result in lower V_p and K_S at ambient pressure and 300 K compared to the linear hydration effects observed in previous studies (Fig. 9) (Meister et al. 1980; Suito et al. 1992; Malfait et al. 2011; Whittington et al. 2012). Using these previously determined linear hydration effects to estimate H_2O_t from seismic measurements would thus result in overestimation of H_2O_t in rhyolitic melts. At high temperatures, however, there are several factors that may affect the nonlinear hydration effects reported here. For instance, the effects of temperature on water speciation can be significant at magmatic temperatures (~ 650 – 800 °C): the ratio of OH^- to H_2O_m will increase dramatically compared to that at ambient temperature (Keppler and Bagdassarov 1993; Nowak

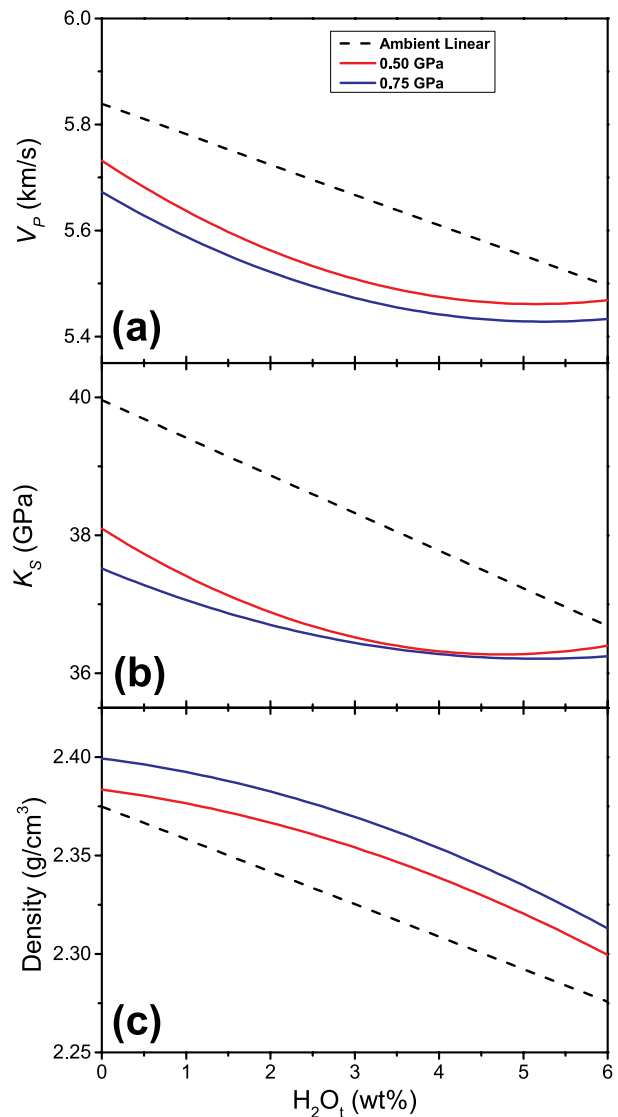


FIGURE 9. Modeled compressional wave velocities, bulk moduli, and density of hydrous glasses at pressures relevant to magmatic processes. (a) Compressional wave velocities, (b) bulk moduli, and (c) densities of rhyolitic glasses as functions of H_2O_t . Solid lines are parabolic fits of the velocity and equation of state parameters at each given pressure. Dashed lines represent linear fits to ambient pressure literature data for rhyolitic glasses from this study, Meister et al. (1980), Suito et al. (1992), and Whittington et al. (2012). (Color online.)

and Behrens 1995; Evans et al. 2016). In contrast, the effects of pressure on altering water speciation at high temperatures up to ~ 2 GPa appear to be negligible (Shen and Keppler 1995; Sowerby and Keppler 1999; Behrens and Yamashita 2008; Chertkova and Yamashita 2015). Because OH^- affects acoustic velocities and elastic moduli more than H_2O_m , such an increase in the ratio of OH^- to H_2O_m at high temperatures may increase velocity reductions in hydrous melts at high P - T and could accentuate the nonlinear effects of H_2O_t found in this study. Furthermore, silicate liquids are expected to be more compressible than their

glass counterparts (Xu et al. 2018). The role of H_2O_m in interstitial voids may thus be enhanced in melts. Such effects could also add to the nonlinear hydration effects at high pressures observed here but should not be too significant at pressures relevant to rhyolitic magma chambers (~0.5 GPa) (Huang et al. 2015; Flinders et al. 2018; Schmandt et al. 2019). In addition to the effects of water on acoustic velocities at high P - T , the direct effects of temperature on acoustic velocities in glasses and melts with varying H_2O_i need to be determined at high- P - T conditions in future studies. Taking all these factors into consideration, it is conceivable that the nonlinear effects of hydration on acoustic velocities and elastic moduli of silicate melts exist in felsic magma chambers at deep crustal conditions. This, in turn, can significantly affect our understanding of seismic signatures and the dynamic behavior of felsic magmas. Despite their geologic significance, the effects of hydration on sound velocities and elastic moduli have yet to be explored at high temperatures, even at ambient pressure. It is thus essential for future studies to examine the combined effects of pressure, temperature, and H_2O on acoustic velocities and elastic moduli in felsic silicate melts at deep crustal conditions.

FUNDING

J.-F. Lin and J.T. Gu acknowledge support from the National Science Foundation (NSF) Geophysics Program (EAR-1916941), NSF Research Experience for Undergraduate Students (REU), and the International Joint Usage Program at the Institute for Planetary Materials. J.E. Gardner acknowledges support from NSF grant EAR-1725186 and T. Okuchi acknowledges support from JSPS KAKENHI (17H01172).

REFERENCES CITED

- Amin, S.A., Rissi, E.N., McKiernan, K., and Yarger, J.L. (2012) Determining the equation of state of amorphous solids at high pressure using optical microscopy. *Review of Scientific Instruments*, 83, 033702.
- Ardia, P., Di Muro, A., Giordano, D., Massare, D., Sanchez-Valle, C., and Schmidt, M.W. (2014) Densification mechanisms of haplogranite glasses as a function of water content and pressure based on density and Raman data. *Geochimica et Cosmochimica Acta*, 138, 158–180.
- Bailey, R.A., Dalrymple, G.B., and Lanphere, M.A. (1976) Volcanism, structure, and geochronology of Long Valley Caldera, Mono County, California. *Journal of Geophysical Research*, 81, 725–744.
- Behrens, H., and Yamashita, S. (2008) Water speciation in hydrous sodium tetrasilicate and hexasilicate melts: Constraint from high temperature NIR spectroscopy. *Chemical Geology*, 256, 306–315.
- Behrens, H., and Zhang, Y. (2001) Ar diffusion in hydrous silicic melts: Implications for volatile diffusion mechanisms and fractionation. *Earth and Planetary Science Letters*, 192, 363–376.
- Birch, F. (1978) Finite strain isotherm and velocities for single-crystal and polycrystalline NaCl at high pressures and 300°K. *Journal of Geophysical Research*, 83, 1257.
- Borg, L.E., and Clyne, M.A. (1998) The petrogenesis of felsic calc-alkaline magmas from the southernmost Cascades, California: Origin by partial melting of basaltic lower crust. *Journal of Petrology*, 39, 1197–1222.
- Brandmeier, M., and Wörner, G. (2016) Compositional variations of ignimbrite magmas in the Central Andes over the past 26 Ma—A multivariate statistical perspective. *Lithos*, 262, 713–728.
- Carn, S.A., Pallister, J.S., Lara, L., Ewert, J.W., Watt, S., Prata, A.J., Thomas, R.J., and Villarosa, G. (2009) The unexpected awakening of Chaitén Volcano, Chile. *Eos, Transactions American Geophysical Union*, 90, 205–206.
- Chertkova, N., and Yamashita, S. (2015) In situ spectroscopic study of water speciation in the depolymerized $Na_2Si_2O_5$ melt. *Chemical Geology*, 409, 149–156.
- Clark, A.N., Leshner, C.E., Jacobsen, S.D., and Sen, S. (2014) Mechanisms of anomalous compressibility of vitreous silica. *Physical Review B—Condensed Matter and Materials Physics*, 90, 1–6.
- Clark, A.N., Leshner, C.E., Jacobsen, S.D., and Wang, Y. (2016) Anomalous density and elastic properties of basalt at high pressure: Reevaluating of the effect of melt fraction on seismic velocity in the Earth's crust and upper mantle. *Journal of Geophysical Research: Solid Earth*, 121, 4232–4248.
- Coasne, B., Weigel, C., Polian, A., Kint, M., Rouquette, J., Haines, J., Foret, M., Vacher, R., and Rufflé, B. (2014) Poroelastic theory applied to the adsorption-induced deformation of vitreous silica. *Journal of Physical Chemistry B*, 118, 14519–14525.
- Crossweller, H.S., Arora, B., Brown, S.K., Cottrell, E., Deligne, N.I., Guerrero, N.O., Hobbs, L., Kiyosugi, K., Loughlin, S.C., Lowndes, J., and others. (2012) Global database on large magnitude explosive volcanic eruptions (LaMEVE). *Journal of Applied Volcanology*, 1, 4.
- Deschamps, T., Martinet, C., Brunel, J.L., and Champagnon, B. (2011) Soda-lime silicate glass under hydrostatic pressure and indentation: A micro-Raman study. *Journal of Physics Condensed Matter*, 23, 035402.
- Dewaele, A., Torrent, M., Loubeyre, P., and Mezouar, M. (2008) Compression curves of transition metals in the Mbar range: Experiments and projector augmented-wave calculations. *Physical Review B*, 78, 104102.
- Evans, B.W., Hildreth, W., Bachmann, O., and Scaillet, B. (2016) In defense of magnetite-ilmenite thermometry in the Bishop Tuff and its implication for gradients in silicic magma reservoirs. *American Mineralogist*, 101, 469–482.
- Flinders, A.F., and Shen, Y. (2017) Seismic evidence for a possible deep crustal hot zone beneath Southwest Washington. *Scientific Reports*, 7, 1–10.
- Flinders, A.F., Shelly, D.R., Dawson, P.B., Hill, D.P., Tripoli, B., and Shen, Y. (2018) Seismic evidence for significant melt beneath the Long Valley. *Geology*, 46, 799–802.
- Fu, S., Yang, J., and Lin, J.-F. (2017) Abnormal elasticity of single-crystal magnesiosiderite across the spin transition in Earth's lower mantle. *Physical Review Letters*, 118, 036402.
- Gardner, J.E., and Ketcham, R.A. (2011) Bubble nucleation in rhyolite and dacite melts: Temperature dependence of surface tension. *Contributions to Mineralogy and Petrology*, 162, 929–943.
- Grove, T.L., Till, C.B., and Krawczynski, M.J. (2012) The role of H_2O in subduction zone magmatism. *Annual Review of Earth and Planetary Sciences*, 40, 413–439.
- Guo, X., Chen, Q., and Ni, H.W. (2016) Electrical conductivity of hydrous silicate melts and aqueous fluids: Measurement and applications. *Science China Earth Sciences*, 59, 889–900.
- Helwig, W., Soignard, E., and Tyburczy, J.A. (2016) Effect of water on the high-pressure structural behavior of anorthite-diopside eutectic glass. *Journal of Non-Crystalline Solids*, 452, 312–319.
- Hess, K.U., and Dingwell, D.B. (1996) Viscosities of hydrous leucogranitic melts: A non-Arrhenian model. *American Mineralogist*, 81, 1297–1300.
- Huang, H.-H., Lin, F.-C., Schmandt, B., Farrell, J., Smith, R.B., and Tsai, V.C. (2015) The Yellowstone magmatic system from the mantle plume to the upper crust. *Science*, 348, 773–776.
- Hui, H., and Zhang, Y. (2007) Toward a general viscosity equation for natural anhydrous and hydrous silicate melts. *Geochimica et Cosmochimica Acta*, 71, 403–416.
- Hui, H., Zhang, Y., Xu, Z., and Behrens, H. (2008) Pressure dependence of the speciation of dissolved water in rhyolitic melts. *Geochimica et Cosmochimica Acta*, 72, 3229–3240.
- Ihinger, P.D., Zhang, Y., and Stolper, E.M. (1999) The speciation of dissolved water in rhyolitic melt. *Geochimica et Cosmochimica Acta*, 63, 3567–3578.
- Keppeler, H., and Bagdassarov, N.S. (1993) High-temperature FTIR spectra of H_2O in rhyolite melt to 1300 °C. *American Mineralogist*, 78, 1324–1327.
- Kimura, J.-I., Nagahashi, Y., Satoguchi, Y., and Chang, Q. (2015) Origins of felsic magmas in Japanese subduction zone: Geochemical characterizations of tephra from caldera-forming eruptions <5 Ma. *Geochemistry, Geophysics, Geosystems*, 16, 2147–2174.
- Kushiro, I., Yoder, H.S., and Nishikawa, M. (1968) Effect of water on the melting of enstatite. *Geological Society of America Bulletin*, 79, 1685–1692.
- Lee, S.K., and Stebbins, J.F. (2009) Effects of the degree of polymerization on the structure of sodium silicate and aluminosilicate glasses and melts: An ^{17}O NMR study. *Geochimica et Cosmochimica Acta*, 73, 1109–1119.
- Lee, S.K., Cody, G.D., Fei, Y., and Mysen, B.O. (2004) Nature of polymerization and properties of silicate melts and glasses at high pressure. *Geochimica et Cosmochimica Acta*, 68, 4189–4200.
- Lee, S.K., Lin, J.-F., Cai, Y.Q., Hiraoka, N., Eng, P.J., Okuchi, T., Mao, H.-k., Meng, Y., Hu, M.Y., Chow, P., and others. (2008) X-ray Raman scattering study of $MgSiO_3$ glass at high pressure: Implication for triclustered $MgSiO_3$ melt in Earth's mantle. *Proceedings of the National Academy of Sciences*, 105, 7925–7929.
- Lee, S.K., Yi, Y.S., Cody, G.D., Mibe, K., Fei, Y., and Mysen, B.O. (2011) Effect of network polymerization on the pressure-induced structural changes in sodium aluminosilicate glasses and melts: ^{27}Al and ^{17}O solid-state NMR study. *Journal of Physical Chemistry C*, 116, 2183–2191.
- Lin, C.C., and Liu, L.G. (2006) Composition dependence of elasticity in aluminosilicate glasses. *Physics and Chemistry of Minerals*, 33, 332–346.
- Liu, J., and Lin, J.-F. (2014) Abnormal acoustic wave velocities in basaltic and (Fe,Al)-bearing silicate glasses at high pressures. *Geophysical Research Letters*, 41, 8832–8839.
- Lowenstern, J.B. (1994) Dissolved volatile concentrations in an ore-forming magma. *Geology*, 22(10), 893–896.
- Lu, C., Mao, Z., Lin, J.-F., Zhuravlev, K.K., Tkachev, S.N., and Prakapenka, V.B. (2013) Elasticity of single-crystal iron-bearing pyrope up to 20GPa and 750K. *Earth and Planetary Science Letters*, 361, 134–142.

- Malfait, W.J., Sanchez-Valle, C., Ardia, P., Médard, E., and Lerch, P. (2011) Compositional dependent compressibility of dissolved water in silicate glasses. *American Mineralogist*, 96, 1402–1409.
- Malfait, W.J., Verel, R., Ardia, P., and Sanchez-Valle, C. (2012) Aluminum coordination in rhyolite and andesite glasses and melts: Effect of temperature, pressure, composition and water content. *Geochimica et Cosmochimica Acta*, 77, 11–26.
- Malfait, W.J., Seifert, R., and Sanchez-Valle, C. (2014) Densified glasses as structural proxies for high-pressure melts: Configurational compressibility of silicate melts retained in quenched and decompressed glasses. *American Mineralogist*, 99, 2142–2145.
- McIntosh, I.M., Nichols, A.R.L., Tani, K., and Llewellyn, E.W. (2017) Accounting for the species dependence of the 3500 cm^{-1} H_2O infrared molar. *American Mineralogist*, 102, 1677–1689.
- Meister, R., Robertson, E.C., Werre, R.W., and Raspet, R. (1980) Elastic moduli of rock glasses under pressure to 8 kilobars and geophysical implications. *Journal of Geophysical Research*, 85, 6461–6470.
- Moore, G., Vennemann, T., and Carmichael, I.S.E. (1995) Solubility of water in magmas to 2 kbar. *Geology*, 23, 1099.
- Mysen, B.O., and Richet, P. (2005) Silicate glasses and melts: Properties and structure. Elsevier Science.
- Newman, S., Stolper, E.M., and Epstein, S. (1986) Measurement of water in rhyolitic glasses: Calibration of an infrared spectroscopic technique vacuum extraction technique. The grain size of the crushed samples can significantly affect. *American Mineralogist*, 71, 1527–1541.
- Ni, H., Keppler, H., Manthilake, M.A.G.M., and Katsura, T. (2011) Electrical conductivity of dry and hydrous $\text{NaAlSi}_3\text{O}_8$ glasses and liquids at high pressures. *Contributions to Mineralogy and Petrology*, 162, 501–513.
- Nowak, M., and Behrens, H. (1995) The speciation of water in haplogranitic glasses and melts determined by in situ near-infrared spectroscopy. *Geochimica et Cosmochimica Acta*, 59, 3445–3450.
- Ochs, F.A., and Lange, R.A. (1999) The density of hydrous magmatic liquids. *Science*, 283, 1314–1317.
- Richet, P., and Polian, A. (1998) Water as a dense icelike component in silicate glasses. *Science*, 281, 396–398.
- Richet, P., Lejeune, A.-M., Holtz, F., and Roux, J. (1996) Water and the viscosity of andesite melts. *Chemical Geology*, 128, 185–197.
- Richet, P., Whittington, A., Holtz, F., Behrens, H., Ohlhorst, S., and Wilke, M. (2000) Water and the density of silicate glasses. *Contributions to Mineralogy and Petrology*, 138, 337–347.
- Sakamaki, T., Kono, Y., Wang, Y., Park, C., Yu, T., Jing, Z., and Shen, G. (2014) Contrasting sound velocity and intermediate-range structural order between polymerized and depolymerized silicate glasses under pressure. *Earth and Planetary Science Letters*, 391, 288–295.
- Sanchez-Valle, C., and Bass, J.D. (2010) Elasticity and pressure-induced structural changes in vitreous MgSiO_3 -enstatite to lower mantle pressures. *Earth and Planetary Science Letters*, 295, 523–530.
- Schmandt, B., Jiang, C., and Farrell, J. (2019) Seismic perspectives from the western U.S. on magma reservoirs underlying large silicic calderas. *Journal of Volcanology and Geothermal Research*, 384, 158–178.
- Seifert, F.A., Mysen, B.O., and Virgo, D. (1981) Structural similarity of glasses and melts relevant to petrological processes. *Geochimica et Cosmochimica Acta*, 45, 1879–1884.
- Shaw, H.R. (1963) Obsidian- H_2O viscosities at 1000 and 2000 bars in the temperature range 700° to 900 °C. *Journal of Geophysical Research*, 68, 6337–6343.
- (1972) Viscosities of magmatic silicate liquids; an empirical method of prediction. *American Journal of Science*, 272, 870–893.
- Shen, A., and Keppler, H. (1995) Infrared spectroscopy of hydrous silicate melts to 1000°C and 10 kbar: Direct observation of H_2O speciation in a diamond-anvil cell. *American Mineralogist*, 80, 1335–1338.
- Shen, G., Mei, Q., Prakashenka, V.B., Lazor, P., Sinogeikin, S., Meng, Y., and Park, C. (2011) Effect of helium on structure and compression behavior of SiO_2 glass. *Proceedings of the National Academy of Sciences*, 108, 6004–6007.
- Sowerby, J.R., and Keppler, H. (1999) Water speciation in rhyolitic melt determined by in-situ infrared spectroscopy. *American Mineralogist*, 84, 1843–1849.
- Stolper, E. (1982a) The speciation of water in silicate melts. *Geochimica et Cosmochimica Acta*, 46, 2609–2620.
- (1982b) Water in silicate glasses: An infrared spectroscopic study. *Contributions to Mineralogy and Petrology*, 81, 1–17.
- Suito, K., Miyoshi, M., Sasakura, T., and Fujisaw, H. (1992) Elastic properties of obsidian, vitreous SiO_2 , and vitreous GeO_2 under high pressure up to 6 GPa. In *High-Pressure Research: Application to Earth and Planetary Sciences*, 67, 219–225.
- Wallace, P.J. (2005) Volatiles in subduction zone magmas: Concentrations and fluxes based on melt inclusion and volcanic gas data. *Journal of Volcanology and Geothermal Research*, 140, 217–240.
- Wallace, P.J., Anderson, A.T., and Davis, A.M. (1999) Gradients in H_2O , CO_2 , and exsolved gas in a large-volume silicic magma system: Interpreting the record preserved in melt inclusions from the Bishop Tuff. *Journal of Geophysical Research: Solid Earth*, 104, 20,097–20,122.
- Wang, Y., Sakamaki, T., Skinner, L.B., Jing, Z., Yu, T., Kono, Y., Park, C., Shen, G., Rivers, M.L., and Sutton, S.R. (2014) Atomistic insight into viscosity and density of silicate melts under pressure. *Nature Communications*, 5, 3241.
- Weigel, C., Polian, A., Kint, M., Rufflé, B., Foret, M., and Vacher, R. (2012) Vitreous silica distends in helium gas: Acoustic versus static compressibilities. *Physical Review Letters*, 109, 1–5.
- Whittington, A., Richet, P., and Holtz, F. (2000) Water and the viscosity of depolymerized aluminosilicate melts. *Geochimica et Cosmochimica Acta*, 64, 3725–3736.
- Whittington, A.C., Richet, P., and Polian, A. (2012) Water and the compressibility of silicate glasses: A Brillouin spectroscopic study. *American Mineralogist*, 97, 455–467.
- Williams, Q., and Jeanloz, R. (1998) Spectroscopic evidence for pressure-induced coordination changes in silicate glasses and melts. *Science*, 239, 902–905.
- Withers, A.C., and Behrens, H. (1999) Temperature-induced changes in the NIR spectra of hydrous albitic and rhyolitic glasses between 300 and 100 K. *Physics and Chemistry of Minerals*, 27, 119–132.
- Withers, A.C., Zhang, Y., and Behrens, H. (1999) Reconciliation of experimental results on H_2O speciation in rhyolitic glass using in-situ and quenching techniques. *Earth and Planetary Science Letters*, 173, 343–349.
- Xu, M., Jing, Z., Chantel, J., Jiang, P., Yu, T., and Wang, Y. (2018) Ultrasonic velocity of diopside liquid at high pressure and temperature: constraints on velocity reduction in the upper mantle due to partial melts. *Journal of Geophysical Research: Solid Earth*, 123, 8676–8690.
- Yang, J., Mao, Z., Lin, J.F., and Prakashenka, V.B. (2014) Single-crystal elasticity of the deep-mantle magnesite at high pressure and temperature. *Earth and Planetary Science Letters*, 392, 292–299.
- Yokoyama, A., Matsui, M., Higo, Y., Kono, Y., Irfune, T., and Funakoshi, K. (2010) Elastic wave velocities of silica glass at high temperatures and high pressures. *Journal of Applied Physics*, 107, 123530.
- Zha, C.-S., Hemley, R.J., Mao, H., Duffy, T.S., and Meade, C. (1994) Acoustic velocities and refractive index of SiO_2 glass to 57.5 GPa by Brillouin scattering. *Physical Review B*, 50, 13,105–13,112.
- Zhang, Y., Belcher, R., Ihinger, P.D., Wang, L., Xu, Z., and Newman, S. (1997) New calibration of infrared measurement of dissolved water in rhyolitic glasses. *Geochimica et Cosmochimica Acta*, 61, 3089–3100.

MANUSCRIPT RECEIVED MAY 12, 2020

MANUSCRIPT ACCEPTED SEPTEMBER 27, 2020

MANUSCRIPT HANDLED BY SERGIO SPEZIALE

Endnote:

¹Deposit item AM-21-77597, Online Material. Deposit items are free to all readers and found on the MSA website, via the specific issue's Table of Contents (go to http://www.minsocam.org/MSA/AmMin/TOC/2021/Jul2021_data/Jul2021_data.html).